Journal of Non-Crystalline Solids 494 (2018) 40–49

Contents lists available at ScienceDirect

Journal of Non-Crystalline Solids

journal homepage: www.elsevier.com/locate/jnoncrysol

Dynamic damage and fracture of a conductive glass under high-rate compression: A synchrotron based study

Z.D. Feng[a,b], Y.H. Zhou[a,b], R. Tan[a,b], H.M. Hou[a,b], T. Sun[c], K. Fezzaa[c], J.Y. Huang[b,*], S.N. Luo[a,b,*]

[a] Key Laboratory of Advanced Technologies of Materials, Ministry of Education, Southwest Jiaotong University, Chengdu, Sichuan 610031, PR China
[b] The Peac Institute of Multiscale Sciences, Chengdu, Sichuan 610031, PR China
[c] Advanced Photon Source, Argonne National Laboratory, Argonne, IL 60439, USA

ARTICLE INFO

Keywords:
Dynamic fracture
Conductive glass
X-ray imaging
Damage quantification

ABSTRACT

Dynamic damage and fracture of conductive glass are investigated using a split Hopkinson pressure bar, implemented with *in situ* X-ray phase contrast imaging (XPCI) and optical imaging for comparison. Quantitative comparison between X-ray and optical images demonstrates that XPCI exhibits much higher resolution in resolving micro cracks and dynamic fracture modes. Multiple predamage and fracture modes of glass samples under dynamic loading are revealed with XPCI to depend on competing nucleation of initial flaws across scales, which give rise to a scattered fracture strength distribution. The fracture strengths increase with increasing strain rates due to accelerated crack propagation and damage growth. Quantitative gray-scale statistical analysis of XPCI and optical images yields spatial and temporal evolutions of damage. Unexpected plateaus essentially without damage growth are observed on the damage curves of glass, deviating from conventional theoretical predictions. The damage plateaus are attributed to growth, closure and re-expansion of inclined main cracks, due to interactions of stress waves with crack tips. The current results also demonstrate a reliable experimental technique for dynamic damage characterization of brittle materials.

1. Introduction

Dynamic fracture and fragmentation of glasses are commonly encountered in a number of engineering applications and are of considerable scientific/industrial interest [1]. Indium tin oxide (ITO) coated glass is frequently used as electrical components such as touch screens and electrodes [2]. Understanding impact-induced deformation, damage and fracture of ITO glass, including phenomena and underlying mechanisms, is critical for better impact resistance, and long-term reliability of electronic devices, but this subject has rarely been touched. Previous studies concerning ITO glass are mainly concentrated on optical and electrical properties of ITO films [3,4].

Extensive efforts have been devoted to compression fracture of commonly-used (e.g. borosilicate, soda-lime, bulk metallic) glasses [5-8]. The rate sensitivity of bulk metallic glass has been fully investigated, while it remains to be clarified for silica-based glasses due to the lack of strength data under high-rate compression (e.g. $> 1000\,s^{-1}$). A number of researchers [6,9-11] have discussed rate-dependency of soda-lime and borosilicate glasses but based on results of only two strain rates. Zhang et al. [12] demonstrated that there exists a critical strain rate beyond which the annealed soda-lime glass exhibits high rate-dependency, similar to the ceramics [13]. Therefore, more dynamic tests are deemed necessary to better understand the non-linear rate effects of silica-based glasses and underlying mechanisms. In addition, the existing flaws play an important role in the fracture of brittle materials. The edge flaws are frequently encountered in glass samples during machining and handling [14,15], which are responsible for the scatter in fracture strengths. However, effects of edge flaws on the dynamic fracture strength of glasses have not been fully investigated.

Compared to fracture strengths, the fracture modes, especially under impact loading, did not receive adequate attention. The crack density under quasi-static fracture is generally lower than that under dynamic loading, and the fracture modes can be distinguished with conventional optical imaging [16,17] and controlled postmortem SEM analysis [7,18]. However, the fracture process under impact loading is highly transient, and it is much more difficult to capture the cracking kinetics (initiation, growth and coalescence) due to motion blur and complex crack interactions. Lamberson et al. [19] studied dynamic fracture of single-crystal quartz with ultrafast optical imaging, and proposed a damage quantification technique based on statistical analysis of high-speed optical images. However, complex interactions of reflected light from microcracks smeared images. The lack of sufficient

* Corresponding authors.
E-mail addresses: jyhuang@pims.ac.cn (J.Y. Huang), sluo@pims.ac.cn (S.N. Luo).

https://doi.org/10.1016/j.jnoncrysol.2018.04.030
Received 25 December 2017; Received in revised form 2 April 2018; Accepted 16 April 2018

spatial resolution hinders the understanding of dynamic fracture modes, and accurate measurement of damage.

Dynamic X-ray phase contrast imaging (XPCI) is proved advantageous for visualizing cracking and fragmentation of brittle materials owing to its edge enhancement, penetration, and high spatial resolution (μm) [20,21]. Parab et al. [22] performed dynamic compression tests on three types of glasses with *in situ* XPCI. The radial and split cracks are resolved clearly in X-ray images. However, the temporal resolution (tens of μs) needs to be improved to capture the detailed fracture process, and quantitative interpretations on damage evolution of glasses remain to be enhanced. Huang et al. [21] investigated dynamic fracture of single crystal silicon and revealed distinct anisotropy in strength properties and fracture modes of Si. XPCI exhibited superiority in visualizing dynamic fracture of nontransparent solids. However, quantitative comparison between X-ray and optical imaging in resolving dynamic fracture kinetics of transparent solids (e.g. glasses) has not been reported.

In the present work, dynamic compression tests are conducted on ITO glass with a split Hopkinson pressure bar (SHPB), while the damage and fracture of glass samples are characterized with *in situ*, high-speed X-ray and optical imaging. Comparison between X-ray and optical images demonstrates that XPCI exhibits much higher resolution in resolving micro cracks and fracture modes. A new technique for damage quantification is proposed based on gray-scale statistical analysis of high-speed X-ray and optical images. Multiple predamage and fracture modes of glass samples under dynamic loading are revealed with XPCI, and provide underlying mechanisms for macroscopic strength responses.

2. Experimental

2.1. Materials and setup

Commercially available ITO glass is chosen as the experimental material. The ITO glass is composed of a 95 ± 10 nm ITO film, and a soda-lime glass substrate. The resistance of the ITO glass is measured as 15–20 Ω. The light transmittance exceeds 85%, indicating excellent transparency. The bulk density of the ITO glass under normal conditions is ~ 2.50×10^3 kg/m^3. The chemical composition (wt %) is SiO_2 (70–73%), CaO (7–12%), Na_2O (7.0%), K_2O (6.0%), Al_2O_3 (1.7–1.9%), MgO (1.0%), Fe_2O_3 (0.05–0.15%), In_2O_3 (1.5%), and SnO_2 (0.15%). The Young's modulus and Poisson's ratio are ~71.6 GPa and ~0.23, respectively, according to the manufacturer. The X-ray diffraction (XRD; PANalytical Empyrean; Cu K_α) pattern of the ITO glass measured from a sample surface in reflection mode is presented in Fig. 1 (a). The X-ray tube is working at 40 kV. The optics configuration is a fixed divergence slit (1/8 °), a fixed incident antiscatter slit (1/2 °), and a PIXcel detector, working in scanning mode with maximum active length. The exposure time is set to 150 s to obtain high signal-to-noise ratio. The main diffraction peaks of ITO film is distributed in a background from the amorphous glass matrix.

The ITO glass is cut into 3 × 3 × 1 mm^3 rectangular plates with a diamond tool. The surface of the sample is manufactured to be mirror finish (waviness ≤0.15 μm/20 mm). Scanning electron microscopy (FEI Quanta 250 FEG-SEM) shows that half-penny flaws (probably form cutting) are distributed randomly along the sample edges (Fig. 1(b)). As illustrated in the figure, the shape factors, length 2*a* and width *c*, of the edge flaws are measured to be 61 ± 26 μm and 23 ± 12 μm, corresponding to an aspect ratio *a*/*c* of 1.45 ± 0.51. The backscattered (BS) image shows no visible compositional difference or heterogeneities across the sample, consistent with the energy dispersive spectroscopy (EDS).

The schematic setup for SHPB loading (1–4), and high-speed X-ray imaging system (6–8) is presented in Fig. 2 (a). The X-ray imaging experiments are conducted at the APS beamline 32-ID-B [23]. Details of the imaging system were presented previously [23]. The sample (5)

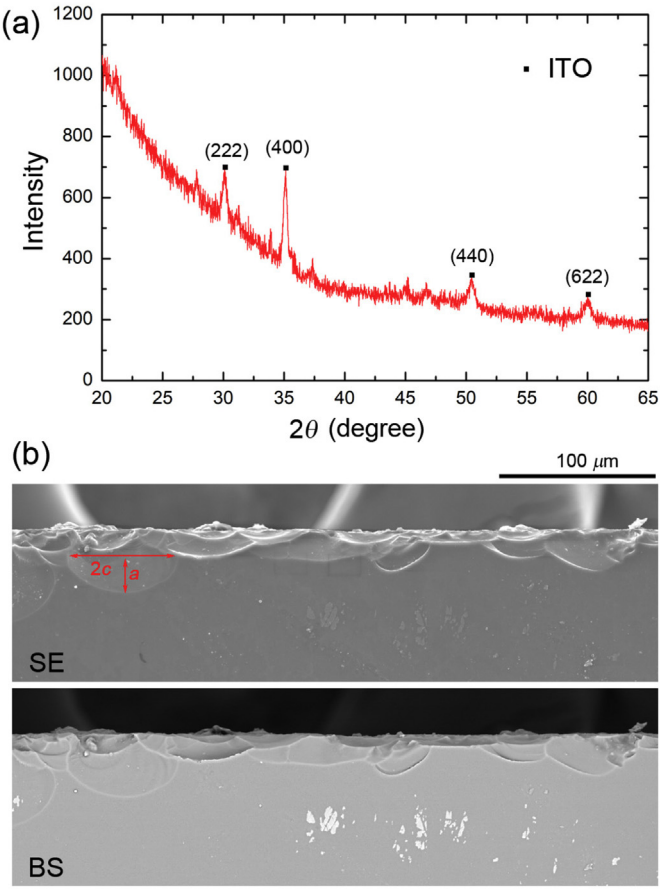

Fig. 1. (a) X-ray diffraction pattern of the ITO glass. (b) SEM images of the edge flaws in the glass sample in a secondary electron mode (SE) and a backscattered mode (BS).

dimensions perpendicular to the incident X-ray beam (the *z*-axis) are 3 ± 0.2 mm × 3 ± 0.2 mm, and the thickness along the view direction is 1 ± 0.1 mm. The striker (1), incident bar (2) and transmission bar (3) of SHPB are all made of high-strength steel with a diameter of 6 mm. After SHPB's gas gun is fired, impact of the striker on the incident bar generates an elastic wave propagating through the incident bar (along the *x*-axis, Fig. 2(a)). A rubber pulse shaper (∅ 3 mm × 0.8 mm) is used to increasing the rising slope of the incident wave [24]. When the incident wave arrives at the interface between the incident bar and the sample (5), it is partially reflected owing to impedance mismatch, while the rest is transmitted into the transmission bar. The incident, reflected and transmitted waves are recorded by strain gauges (4). The transmitted and reflected waves are used to calculate the engineering stress (σ) and strain rate ($\dot{\varepsilon}$) applied to the sample with the two-wave technique [25], and

$$\sigma_s = -E_b \varepsilon_t \frac{A_b}{A_s}, \tag{1}$$

$$\dot{\varepsilon}_s = -\frac{2C_b \varepsilon_r}{L_s}, \tag{2}$$

where ε is strain, A is cross-sectional area, L is length, and C is sound speed. Subscripts i and r denote the incident and reflection bar, respectively; subscripts b and s denote bar and sample, respectively. In this work, compressional stress and strain are positive.

The raw records of a representative shot are presented in Fig. 2(b). The incident pulse owns a gradually rising slope through pulse shaping. A platform appears in the reflected pulse, indicating an approximately constant-rate loading. Eq. (2) is valid when dynamic stress equilibrium is achieved in the sample subjected to SHPB loading, which requires